

## Article

# Enhanced Tribological Performance of Micro-Beam Plasma-Cladded Ni60 Coatings with Addition of Mo and Ag Lubricants in a Wide Temperature Range

Fuxing Ye <sup>1,2,\*</sup>, Yufeng Zhang <sup>1</sup>, Zhi Lou <sup>1</sup> and Yingfan Wang <sup>1</sup>

<sup>1</sup> Tianjin Key Laboratory of Advanced Joining Technology, School of Materials Science and Engineering, Tianjin University, Tianjin 300072, China; 2021208079@tju.edu.cn (Y.Z.); xjsslz@163.com (Z.L.); 3018208222@tju.edu.cn (Y.W.)

<sup>2</sup> Key Lab of Advanced Ceramics and Machining Technology of Ministry of Education, Tianjin 300072, China

\* Correspondence: yefx@tju.edu.cn

**Abstract:** In recent years, there has been significant attention on the application potential of medium and high-temperature self-lubricating composites as sliding parts in extreme environments. This study examines the effects of different Mo and Ag content on the composition and wear resistance of Ni60-cladded coatings at room temperature, 300 °C and 600 °C, while also analyzing their wear mechanism by studying the tribofilm. The results indicate that with an appropriate weight addition of Mo and Ag, one typical lubricant called Ag<sub>2</sub>MoO<sub>4</sub> emerges. At room temperature, the cladding layer containing 5 wt.% Mo and 5 wt.% Ag exhibits a wear rate of  $2.08 \times 10^{-6}$  mm<sup>3</sup>/Nm, and an average coefficient of friction (COF) of 0.3410. These two are 85% and 11% lower than those of the Ni60 cladding layer, respectively. At 300 °C, MoO<sub>3</sub> and Cr<sub>2</sub>MoO<sub>6</sub> act as solid lubricants. Furthermore, at 600 °C, a MoSi<sub>2</sub> and SiO<sub>2</sub> film forms on the worn surface to prevent further oxidation of MoSi<sub>2</sub> and enhance oxidation resistance. The main wear mechanism is adhesion wear. Under higher temperatures, the newly formed Ag<sub>2</sub>MoO<sub>4</sub> in the composite cladding layer adopts a layered cubic spinel structure where low-energy Ag-O bonds preferentially break during friction processes, demonstrating excellent lubrication performance.



**Citation:** Ye, F.; Zhang, Y.; Lou, Z.; Wang, Y. Enhanced Tribological Performance of Micro-Beam Plasma-Cladded Ni60 Coatings with Addition of Mo and Ag Lubricants in a Wide Temperature Range. *Coatings* **2023**, *13*, 1996. <https://doi.org/10.3390/coatings13121996>

Academic Editor: Csaba Balázsi

Received: 26 October 2023

Revised: 21 November 2023

Accepted: 21 November 2023

Published: 24 November 2023



**Copyright:** © 2023 by the authors. Licensee MDPI, Basel, Switzerland. This article is an open access article distributed under the terms and conditions of the Creative Commons Attribution (CC BY) license (<https://creativecommons.org/licenses/by/4.0/>).

**Keywords:** wide temperature range; Ni-based alloy; Ag<sub>2</sub>MoO<sub>4</sub>; self-lubricating

## 1. Introduction

With the advancement of the modern era and the progress in science and technology, there is a growing demand for improved service conditions for components used in industrial applications [1]. Among various forms of material failure, wear and tear is predominantly responsible for poor component conditions. Lubricating materials play a crucial role in reducing friction and wear, thus finding extensive usage across diverse fields. In highly competitive sectors like aerospace, nuclear industry, and equipment manufacturing, there are emerging requirements for developing and preparing materials with enhanced wear resistance and lubrication capabilities [2]. However, traditional lubricants fail to meet regular operational needs at temperatures exceeding 300 °C; hence, stable chemical solid lubricants become the sole choice for minimizing friction and wear [3]. Various high-temperature solid lubricants exist with complex mechanisms, including (1) soft metals characterized by lower shear strength such as Ag, Au, and Pb [4]; (2) lamellar structures exhibiting weak bonding forces like MoS<sub>2</sub>, WS<sub>2</sub>, and graphite [5]; and (3) metal fluorides and oxides such as CaF<sub>2</sub>, TiO<sub>2</sub>, Ag<sub>2</sub>MoO<sub>4</sub> [6,7].

Solid lubricants offer solutions to challenging lubrication problems encountered in high-tech industries with harsh and complex working environments, such as the aerospace, nuclear, and electric sectors. However, the incorporation of solid lubricants often weakens

the bonding within composites, resulting in reduced durability, shorter service life, and inferior wear resistance. Additionally, they can compromise the strength of composites [8–10]. The primary objective of this research is to develop self-lubricating composite materials that exhibit exceptional wear resistance and tribological characteristics across a wide temperature range. Nickel matrix alloy is renowned for its remarkable attributes, including high strength, excellent antioxidant properties, good wear resistance, and creep strength, as well as enduring resilience against gas corrosion [11–13]. The excellent all-around properties of these alloys find wide applications in the aerospace, shipbuilding, and automotive communication industries. There has been extensive research conducted on Ni-based high-temperature solid lubrication composites. Numerous scholars have investigated the impact of combining solid lubricants with nickel-based alloys on the tribological properties of self-lubricating materials [14]. Li Jianliang et al. fabricated molybdenum layers on silver nickel-based alloys using double glow plasma surface alloying technology. They found that after molybdenized, the COF of silver-containing nickel-based alloys decreased by more than 30%, and the wear rate at high temperatures decreased [15]. Huang XinYang et al. fabricated WC-Ni-Cr-based self-lubricating composites containing WS<sub>2</sub> in different temperature and pressure conditions via pulsed electric current sintering. They analyzed the test results and the morphologies of polished surfaces and wear traces and found that, during sliding, WS<sub>2</sub> in the composites would shift to the area in contact with other wear debris to reduce their COF [16]. Ouyang JiaHu et al. fabricated NiCr-BaCr<sub>2</sub>O<sub>4</sub> composites using the hot-pressing method and found that Cr<sup>6+</sup> in BaCrO<sub>4</sub> formed in the temperature range of 400~800 °C, which could promote the densification of the oxidized glaze layer and finally form a protective glaze layer, effectively reducing the friction and wear at a high temperature [17]. Feng Siping et al. fabricated nickel-based self-lubricating composites containing Ti<sub>3</sub>SiC<sub>2</sub> and Ag<sub>2</sub>W<sub>2</sub>O<sub>7</sub> using powder metallurgy and found that Ag<sub>2</sub>W<sub>2</sub>O<sub>7</sub> decomposed into metallic silver and CrWO<sub>4</sub> during high-temperature preparation, which significantly improved the friction and wear properties of nickel-based composites [18]. However, little research is concerned with self-lubricant generation in situ. Compared to ex situ, the in situ generation method can greatly improve the preparation efficiency and quality of materials and reduce the pollution and waste in the preparation process. Thus, the research on the tribological properties of self-lubricant generation in situ is of great importance. In addition, the formation of different lubricants at varying temperatures enhances their adaptability across a wide temperature range [19,20].

## 2. Materials and Methods

The design concept involves utilizing a Ni60 alloy as the coating substrate and incorporating Mo and Ag elements into the cladding layer to enhance its tribological performance. During the cladding process, Mo serves as a conventional reinforcing element for nickel matrix alloys, exerting a significant solid-solution-strengthening effect. The solid solubility of Mo in Q235 is 3%~4%. Additionally, high-temperature oxidation of Mo can generate molybdenum oxide and molybdate compounds at different temperatures that greatly improve the lubricating properties of high-temperature alloys and adaptability across a wide temperature range. Compared to other non-metallic materials, Ag exhibits superior wettability on the nickel matrix and could improve wear resistance of the coating layer.

The Q235 substrate was selected as the base material for fabricating Ni60–Mo self-lubricating composites using the micro-beam plasma-cladding technique (Tables 1 and 2). The samples with varying compositions were designated as S1–S5.

**Table 1.** Compositions of Ni60 (wt.%).

Element	C	Cr	B	Si	Fe	Ni
Composition	0.78	15.90	1.90	4.55	5.00	balance

**Table 2.** Compositions of cladding layers (wt.%).

No.	Mo	Ni60	Ag
S1	-	100	-
S2	5	95	-
S3	10	90	-
S4	15	85	-
S5	5	90	5

The mechanical alloying process via ball milling was performed with a rotation rate of 500 RPM, a ball–material ratio of 10:1, and positive and negative alternating rotations for two hours. The powder after ball milling was compacted and flattened by placing it into a mold with PVA, resulting in the production of a rectangular powder strip measuring  $50 \times 4 \times 2$  mm. Subsequently, the strip was dried at  $120^\circ\text{C}$  for two hours in an oven for further utilization. The substrates utilized were Q235 steel plates that were machined into dimensions of  $200 \times 50 \times 1.5$  mm using electric spark cutting techniques, and the surface was polished with sandpaper to remove the oxide film, the grease was washed, and the surface was cleaned with alcohol and oven-dried at  $120^\circ\text{C}$  for 1.5 h. To facilitate welding, the prepared powder strip was positioned on the central axis of the substrate surface, and the welding process parameters were set as shown in Table 3. The experiment utilized a trans TIG 800 welding power supply manufactured by Fronius company (Wels, Austria), and the Plasma Module 10 was employed as a micro-beam plasma arc generator. The transTig is a completely digitized TIG DC power source with a welding current from 0.5 A to 80 A.

**Table 3.** Cladding process parameters.

Welding Velocity $v/(\text{mm}\cdot\text{s}^{-1})$	Current I/A	Shielding Gas Flow $F/(\text{L}\cdot\text{min}^{-1})$	Plasma Gas Pressure P/(MPa)
0.6	30	15	0.4

The friction and wear experiments on the cladding layer were conducted at room temperature using the UMT-Tribolab reciprocal sliding friction and wear testing apparatus provided by The Bruker Company (Germany). And the tribological tests parameters are shown in Table 4. The 2D depth of wear marks and their morphology were assessed using the 3D digital microscope. The ball-on-flat linear reciprocating wear test was utilized. The  $\text{Al}_2\text{O}_3$  ball ( $\Phi$  9 mm, HRa 90) was selected to slide against the composite coating as the counter body to avoid the oxidation of friction pairs. The morphology of wear marks was quantified using a 3D digital microscope, enabling the acquisition of data about depth and width, as well as generating a comprehensive 3D cloud image. The micro-hardness of the cladding layer was evaluated using an MH-6L micro-hardness tester.

**Table 4.** Tribological test parameters.

Temperature ( $^\circ\text{C}$ )	Applied Load (N)	Frequency (Hz)	Stroke Length (mm)	Testing Time (min)
25, 300, 600	20	5	10	30

### 3. Results and Discussion

#### 3.1. Microstructures

Figure 1 shows the microstructure morphology and mapping scan results of cladding layer S2~S5. The dark-gray sheet-like compositions primarily consisted of Mo and Cr, while the elongated strip-like compositions are composed mainly of Cr. The solid-solution

effect promoted the facile dissolution of Mo into the chromium layer, which was enriched with a reinforced phase, leading to the formation of a Cr-based solid solution. Mo and Co transferring into the matrix would reinforce the solid solution and form a  $\gamma$ -Ni solid solution in stages. During the initial cooling stage, the first  $\gamma$ -Ni phase was nucleated within the liquid phase and subsequently formed dendrites at the matrix interface. The residual liquid was subsequently discharged, resulting in the enrichment of B, Si, and Cr in the remaining liquid phase. The solidification process resulted in the formation of a Cr-Mo solid solution, as Cr was miscible with Mo. Subsequently, once the remaining content of Cr and B reaches the eutectic point, a binary eutectic compound consisting of chromium and boron continues to be generated. The Si element was further enriched in the remaining liquid phase, resulting in the formation of the binary eutectic compound  $\text{Ni}_2\text{Si}$ .

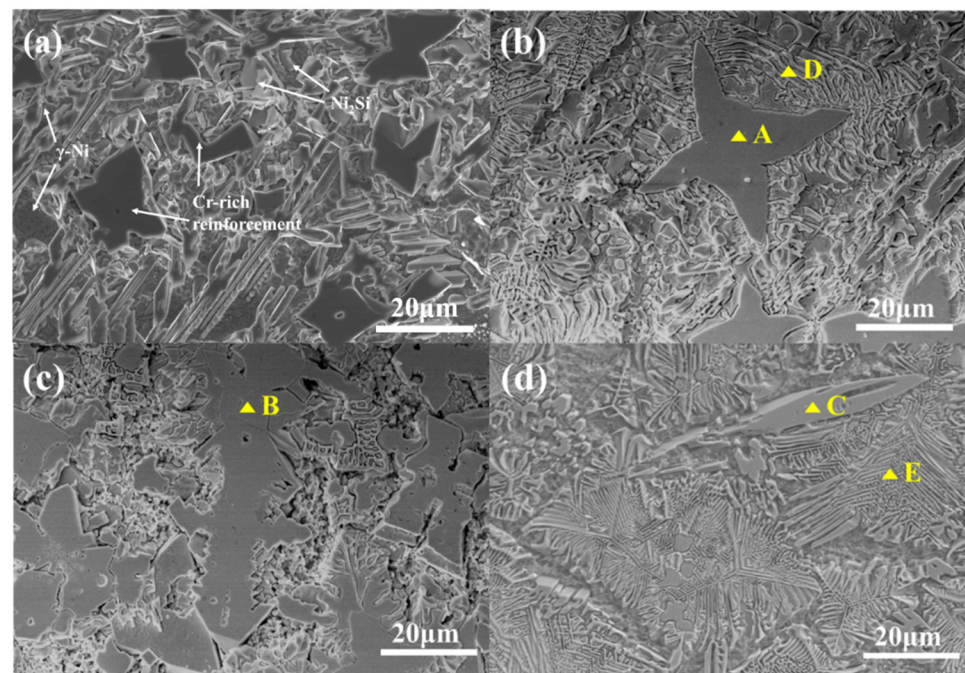


**Figure 1.** Microstructure morphology of S2–S5. (a) S2; (b) S3; (c) S4; (d) S5.

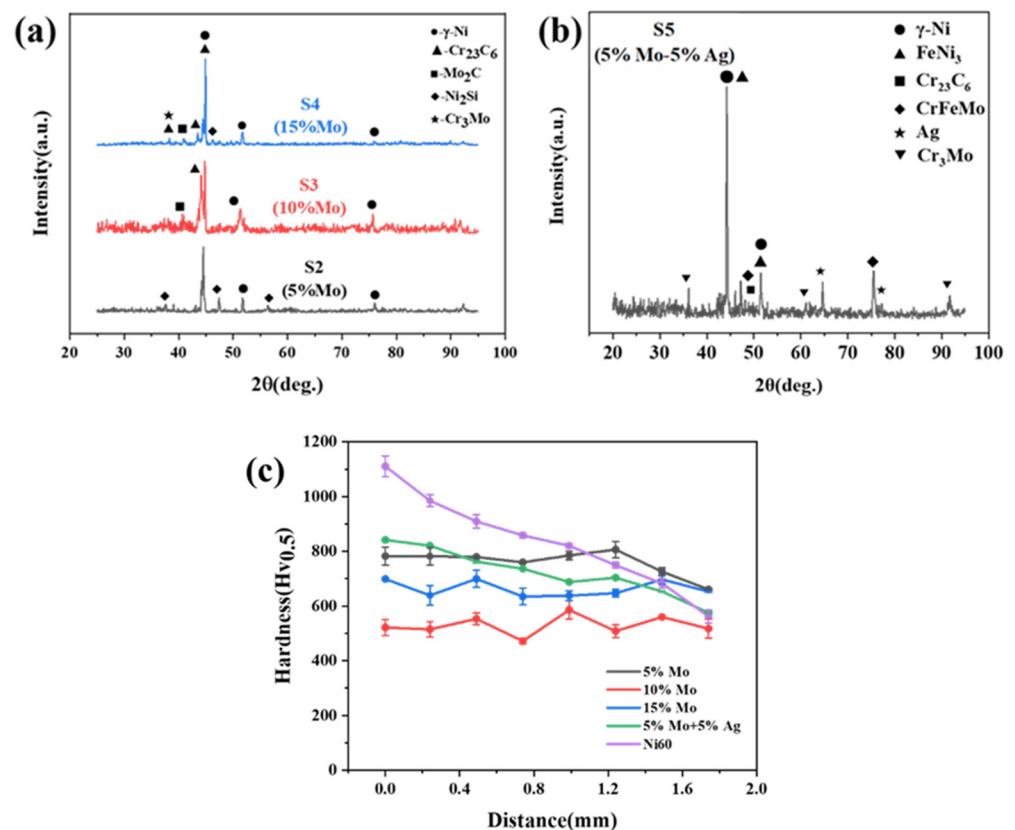
Figure 1b,c shows the microstructure morphologies of cladding layers S3 and S4. The point-scanning composition analysis of different tissues was performed using EDS, and the results are shown in Table 5. It was suggested that the larger dark-gray lamellar tissue A and B in Figure 1b,c is the Cr-rich reinforced phases of solid-solution Mo. The dominant elements in D were primarily Ni, with small quantities of Fe and C. Therefore, it was expected to exhibit a  $\gamma$ -Ni matrix. C had a high content of C and Cr, so it was a Ni-Cr-Fe solid solution. The tissue C, which was a light-gray long strip structure, exhibited a high content of Cr and C corresponding to the  $\text{Cr}_{23}\text{C}_6$ . Point E was skeletal organization, which was supposed to be CrFeMo. It was found that the microstructure and phase distribution are similar under the different ratios. All of them contained a dark-gray lamellar structure and a sunken stream structure. The tissue area gradually increased, and the distribution was more continuous, forming a skeleton and interlinking, and the stream-like tissue was gradually obvious with the increase in Mo content. At the same time, the acicular structure  $\text{Cr}_{23}\text{C}_6$  disappeared and was replaced by a large area of stream structure. The results showed that the addition of Mo changed the shape of the Cr-rich reinforcement phase in the cladding layer, and the Mo element plays the role of solid-solution strengthening.

**Table 5.** EDS scanning results of positions A–E in Figure 1.

Position	Ni	Cr	Fe	Mo	Si	C
A	6.94	36.35	9.34	28.69	-	18.68
B	8.78	32.03	2.63	34.18	-	22.39
C	4.27	41.23	15.87	3.95	-	33.10
D	57.20	4.93	18.28	-	6.92	12.67
E	44.42	16.73	30.35	4.90	3.70	-

The microstructure and phase distribution were found to be similar, consisting of dark-gray tissues resembling sheets and depressed fascicular tissues. Additionally, when Mo rises, the dark-gray tissue region expands progressively, and the distribution becomes more even. The results indicated that the inclusion of Mo in micro-beam plasma cladding may lead to a modification in the geometry of the Cr-rich reinforcing phase in the cladding.

Figure 2 shows the X-ray diffraction (XRD) patterns of the S2–S5 cladding layer. The addition of Mo in the alloy led to the formation of a Mo<sub>2</sub>C-reinforced phase via carbon reaction at elevated temperatures, while another portion dissolved into a Cr-rich hard phase to form a solid solution. In Figure 2b, it could be found that Ag exists as an elementary substance, and Mo formed a solid solution with Cr.

**Figure 2.** XRD patterns of cladding layers. (a) S2–S4; (b) S5; (c) the micro-hardness curves of S2–S5.

### 3.2. Hardness

The micro-hardness curve in Figure 2c represents the top-down analysis of the S2–S5 cladding layer section, revealing that the average hardness of the S2 cladding layer surpasses that of both the S3 and S4 cladding layers, with a relatively moderate fluctuation. The surface hardness of the cladding layer was about 29% lower than that of S1. With the increasing content of Mo, more Mo dissolves in the Cr-rich strengthening phase, or Mo<sub>2</sub>C forms to improve the hardness. However, because of the limited content of the C element in Ni60, when the content of Mo continues to increase, one kind of intermetallic compound

called  $\sigma$  consisting of Co, Cr, and C would be produced at the grain boundary due to the severe deficiency of C in the alloy according to the phase diagram of Co-Cr-C, which had a high brittleness. Its distribution in the tissue led to a decrease in the overall hardness [21].

### 3.3. Tribological Properties

The COF curves of the cladding layers S1~S5 at room temperature are shown in Figure 3a. Table 6 presents the results obtained from calculating the average COF and wear rate of cladding layers. S5 exhibited the lowest COF and wear rate among the five cladding layers. Conversely, S3 exhibited the highest COF of 0.4355 and wear rate of  $27.39 \times 10^{-6} \text{ mm}^3/\text{Nm}$ . The addition of Mo initially increased and subsequently decreased the COF and wear rate, which was slightly higher than that observed for Ni60 without Mo at room temperature, suggesting that incorporating Mo did not contribute to an improvement in tribological properties under such conditions. For S5, its COF remained stable during the first 800 s and then experienced a slight decrease after a small increase, ultimately reaching its minimum value at room temperature. The simultaneous incorporation of both Mo and Ag elements in this study resulted in superior tribological performance under the given conditions.

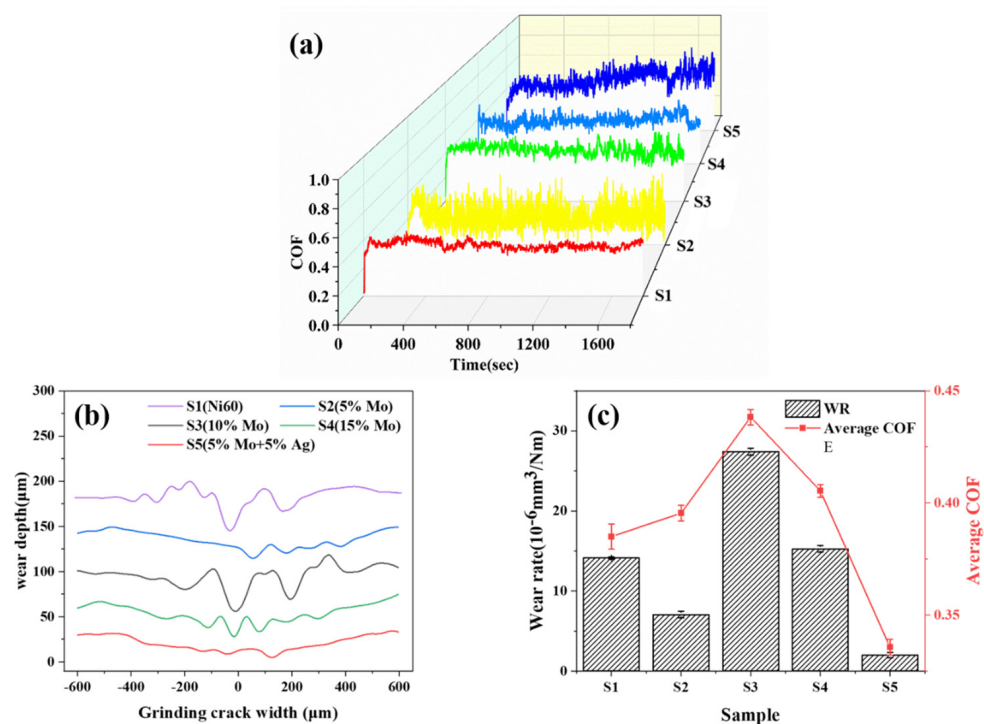


**Figure 3.** (a) COF curves of different samples at 25 °C; (b) S2~S5 2D images of wear scar morphology; (c) average COF and wear rate of S1~S5 at 25 °C.

**Table 6.** Average COF and wear rate ( $\times 10^{-6} \text{ mm}^3/\text{Nm}$ ) of S1~S5 at 25 °C.

No.	S1	S2	S3	S4	S5
Average COF	0.3850	0.4008	0.4355	0.4004	0.3410
Wear rate	14.13	7.060	27.39	15.27	2.080

The cross-sectional morphology of the wear trace of the S1~S5 cladding layer obtained with a 3D digital microscope is depicted in Figure 3b. Analysis of the depth and width variations in the wear trace revealed that the S3 cladding layer exhibits the most severe wear at room temperature, characterized by a higher COF and wear rate. Conversely, the S5 cladding layer demonstrated superior wear resistance performance.

The relationship between wear rate and average COF for each of the S1–S5 cladding layers at room temperature is illustrated in Figure 3c, highlighting the similarities observed between these two parameters. Notably, it was observed that both wear rate and average COF were the highest for the S3 cladding layer while being the lowest for the S5 cladding layer.

The cloud plots of the 3D wear morphology of the S2–S5 cladding layers after sliding friction at room temperature, captured with a 3D digital microscope, are presented in Figure 4. In Figure 4b, significant wear areas and numerous adhesive pits were observed. Weight loss measurements revealed that S3 exhibited the highest weight loss among the four cladding layers tested, indicating its inferior friction performance. Additionally, compared to others, Figure 4d displayed a relatively flat surface, with wear tracks distributed along the sliding direction. The wear mechanism was mainly adhesion wear.

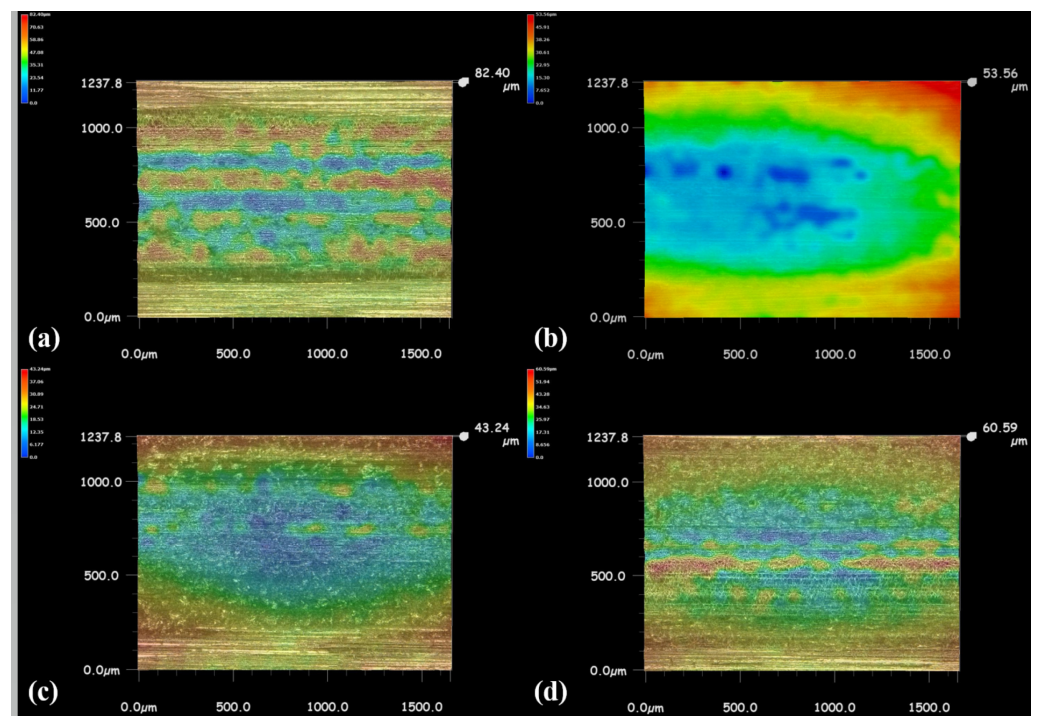


**Figure 4.** The 3D wear morphologies of cladding layers at 25 °C (a) S2; (b) S3; (c) S4; (d) S5.

Figure 5 shows the worn surface morphologies of the S2–S5 cladding layers at room temperature, and the analysis results are shown in Table 7. The lamellar debris observed at points A and B in Figure 5a primarily indicated adhesion wear. Notably, the S3 cladding layer surface depicted in Figure 5b exhibited the most severe signs of wear. There was less wear on the surface of the S5 cladding layer in Figure 5d. Point G represented the elongated white tissue strip exhibiting 83% Ag content aligned with the direction of friction, indicating that Ag aggregated preferentially along this direction due to its relatively low hardness during the frictional process. It circumvented direct contact between the grinding ball and the cladding layer during operation, thereby minimizing the generation of wear particles and debris [22].

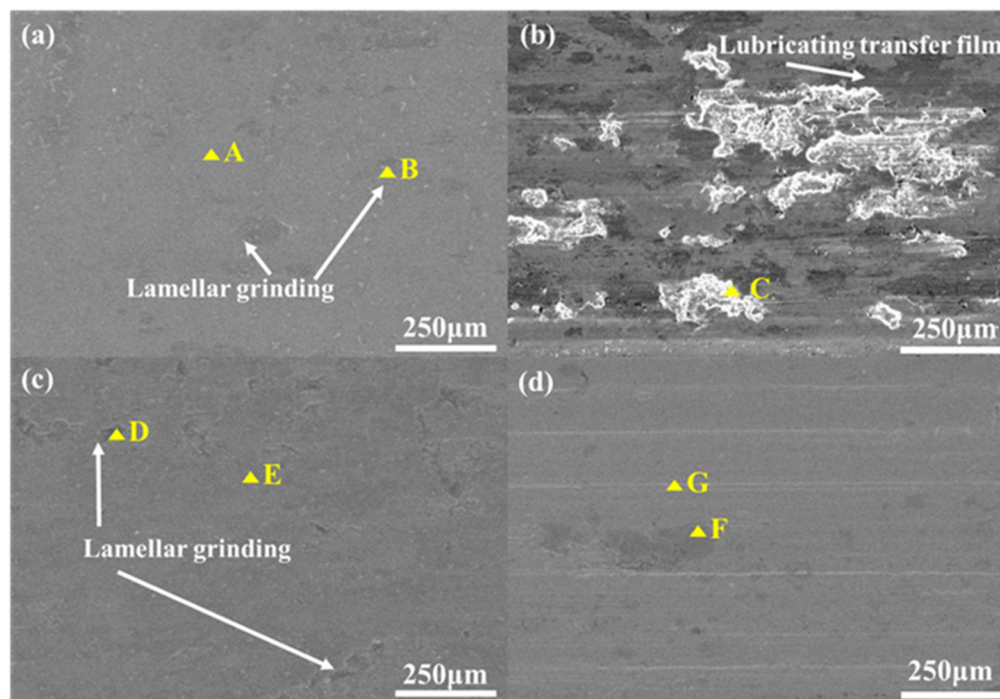


Figure 5. Worn surface morphologies at 25 °C (a) S2; (b) S3; (c) S4; (d) S5.

Table 7. Results of EDS point-scanning results (at. %) in Figure 5.

Position	Ni	Cr	O	Mo	Ag	Al	C	Fe
A	14.851	5.609	17.415	0.581	-	0.358	44.775	16.411
B	24.645	27.201	16.119	1.936	-	1.793	-	28.306
C	50.548	9.215	17.172	1.566	-	0.413	8.565	12.521
D	27.658	13.453	27.825	19.306	-	1.613	-	10.145
E	56.196	17.899	8.037	3.005	-	4.109	-	10.754
F	50.795	9.445	10.701	3.621	4.709	5.102	-	15.629
G	-	7.980	-	2.769	82.615	2.247	-	4.389

To investigate the influence of the simultaneous addition of Mo and Ag on the tribological properties across a wide temperature range, high-temperature friction tests were performed on the S2 and S5 cladding materials. The obtained results for COF and wear rate are presented in Figure 6 and Table 8, revealing slightly superior tribological performance at 300 °C and 600 °C compared to room temperature.

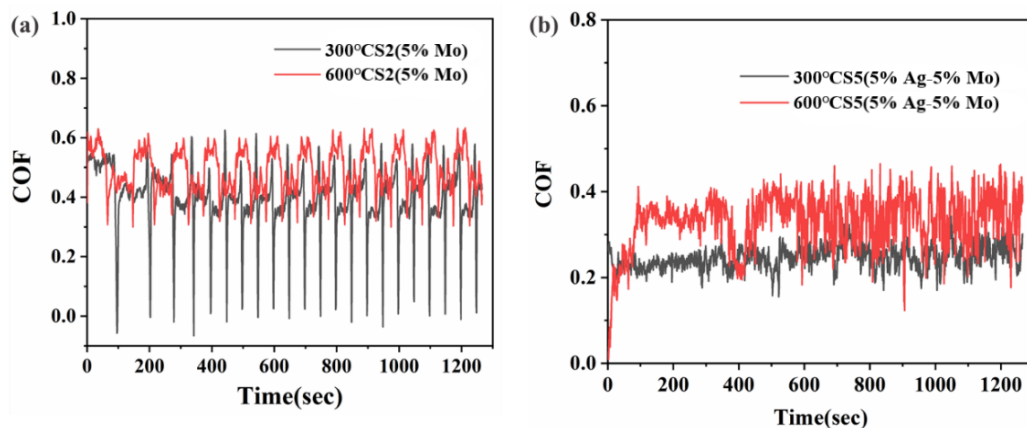


Figure 6. COF curves (a) S2; (b) S5.

**Table 8.** Average COF and wear rate ( $\times 10^{-6}$  mm<sup>3</sup>/Nm) of S2 and S5.

No.	300 °C		600 °C	
	COF	Wear Rate	COF	Wear Rate
S2	0.3970	8.13	0.4921	12.21
S5	0.2464	3.50	0.3319	4.86

Figure 7a–e shows the worn surface morphologies and XRD patterns of the S2 cladding layer at high temperatures. The Figure 7b,d,g,i are magnified within the yellow box on the left. The cladding layer experienced more severe surface squeezing and deformation during the friction process. The surface of cladding layers exhibited friction grooves, as depicted in Figure 7a, accompanied by an extrusion layer featuring a distinct bright white edge. The friction surface of the cladding layer exhibited the formation of black oxide at 600 °C, resulting in more severe wear compared to that observed at 300 °C. During the friction process, wear debris became detached from the surface, thereby leading to an increase in both the wear rate and COF. Upon the magnification of 500, Figure 7d reveals the emergence of a white granular bulge, which was postulated to undergo an oxidation reaction at elevated temperatures, leading to the formation of MoO<sub>3</sub>, Cr<sub>2</sub>MoO<sub>6</sub>, and other oxides based on point-scan analysis [23]. The granular bulge of these oxides, formed at elevated temperatures, led to an increase in adhesion wear at 600 °C.

The XRD phase analysis of the surface after the friction experiment of the S2 cladding layer at 25 °C, 300 °C, and 600 °C is presented in Figure 7e. It was observed that an increase in temperature leads to the appearance of various oxides on the friction surface of cladding layers which were absent at room temperature. At room temperature, the phases present in the cladding layers are  $\gamma$ -Ni and Ni<sub>3</sub>Si<sub>2</sub>. At 300 °C, additional phases including NiO, CrFe<sub>2.32</sub>MoNi, Cr<sub>2</sub>MoO<sub>6</sub>, and MoO<sub>3</sub> were detected. Upon heating to 520 °C in air, Mo underwent slow oxidation, resulting in Mo<sub>2</sub>O<sub>3</sub> being stable at room temperature but oxidizing rapidly to MoO<sub>3</sub> above 600 °C. Furthermore, a new phase of MoSi<sub>2</sub> formed within the cladding layer at 600 °C. In high-temperature environments, the dense and protective SiO<sub>2</sub> film effectively formed on the surface of MoSi<sub>2</sub>, preventing further oxidation due to its low oxygen diffusivity [24]. According to the XRD results, it is supposed that the simplified friction oxidation reaction is

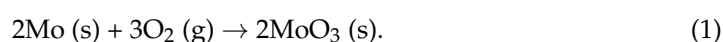
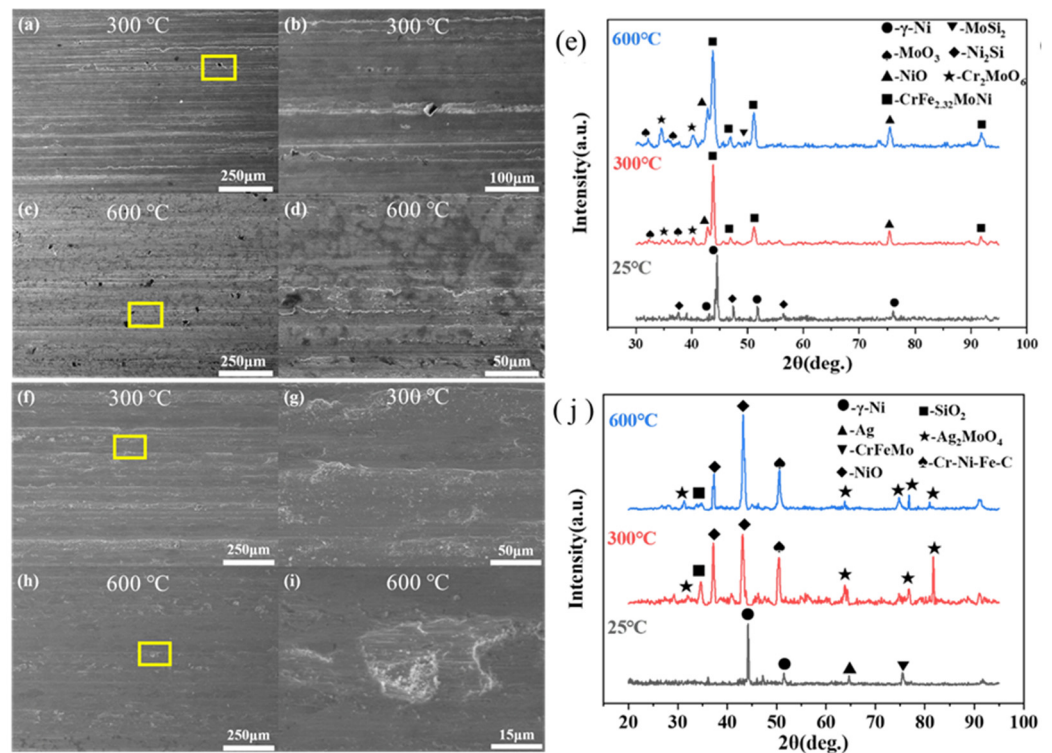
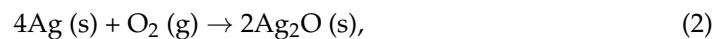


Figure 7f–j shows the worn surface morphologies and XRD patterns of the S5 cladding layer at high temperatures. The primary components detected at room temperature include  $\gamma$ -Ni, FeNi<sub>3</sub>, Cr<sub>23</sub>C<sub>6</sub>, CrFeMo, Ag, and Cr<sub>3</sub>Mo. Notably, Ag was present as an elemental substance, while Mo formed a solid solution with Cr. At 300 °C, NiO, Ag<sub>2</sub>MoO<sub>4</sub>, SiO<sub>2</sub>, and other oxides were also observed on the cladding layer surface. Furthermore, at 600 °C there was an increase in the peak intensity of Ag<sub>2</sub>MoO<sub>4</sub>, which exhibited good stability at high temperatures due to its layered structure with a typical cubic spinel configuration. The unit cell of Ag<sub>2</sub>MoO<sub>4</sub> comprised two fundamental structural units consisting of [AgO<sub>6</sub>] octahedral clusters and [MoO<sub>4</sub>] tetrahedral clusters. During the sliding motion between grinding balls and the composite coating surface layers containing Ag<sub>2</sub>MoO<sub>4</sub> interlayers, it was found that the breaking energy for the Ag-O bond (220 kJ/mol) was significantly lower than that for the Mo-O bond (560 kJ/mol). Consequently, this facilitates the easier break of the Ag-O bond, leading to the formation of a lubricant film enriched with silver that exhibits exceptional lubrication properties [25].



**Figure 7.** (a–d) Worn surface morphologies of S2 (e) XRD patterns of S2. (f–i) Worn surface morphologies of S5 (j) XRD patterns of S5.

Meanwhile, the formation of hard oxides such as NiO not only enhanced the micro-hardness of the coating but also augmented its wear resistance. However, an excessive presence of oxides might create particles, resulting in severe friction-induced wear between mating surfaces. Based on the XRD results, it is reasonable to suppose that the simplified friction oxidation reaction is



According to the analysis, the spontaneity of Equations (2) and (4) was observed at temperatures of 300 °C and 600 °C. The Gibbs free energy was valued for Equation (3) at  $-664.90 \text{ kJ/mol}$  and  $-576.05 \text{ kJ/mol}$  at 300 °C and 600 °C, respectively, indicating the thermodynamic feasibility of the reaction at both temperatures [26].

The self-lubricating mechanism of Mo and Ag composite lubricating materials across a wide temperature range could be described as follows: the formation of oxides such as  $\text{Ag}_2\text{MoO}_4$ ,  $\text{MoO}_3$ , and NiO synergistically lubricated with Ag, resulting in the creation of a dense and smooth film. Due to the lower bond energy between Ag–O during friction,  $\text{Ag}_2\text{MoO}_4$  effectively slid between the layers, exhibiting exceptional lubricating characteristics.

#### 4. Conclusions

The micro-beam plasma-cladding technique was utilized to fabricate Ni-based cladding layers with varying Mo content in this study. The influence of Mo and Ag on the microstructure and tribological characteristics of these Ni-based cladding layers was investigated at different temperatures. The following are the findings:

1. Cladding layers prepared using the micro-beam plasma technique achieved metallurgical bonding with the substrate. This study has potential limitations. We did not take welding defects into full consideration, especially impurities, micro-cracks, and porosities. The presence of welding defects significantly affects the quality of the cladding layer. However, such defects are rarely observed in the cladding layers of micro-beam plasma welding, and the quality of the weld is partly ensured.
2. The coefficient of friction of the coating layer exhibited regular variations at elevated temperatures upon the moderate addition of Mo. At 300 °C, MoO<sub>3</sub> and Cr<sub>2</sub>MoO<sub>6</sub> were formed in S2 as solid lubricants, contributing to high-temperature self-lubrication. However, the generation of MoSi<sub>2</sub> leads to an increase in adhesion wear at 600 °C. The cladding layers exhibited lower COF and wear rate after adding an additional Ag element. The newly formed composite cladding layer underwent a transformation at elevated temperatures, resulting in the development of a layered cubic spinel structure composed of Ag<sub>2</sub>MoO<sub>4</sub>. The preferential break of low-energy Ag-O bonded during the friction process enables excellent lubrication performance through sliding between these layers.
3. Modern aerospace, weapons, and other manufacturing industries have a great demand for mechanical moving parts in a wide temperature range while having good lubricity and wear resistance of the material and its preparation technology. The Ni-based coatings with excellent friction properties and lubrication performance in the study have great potential in these fields, such as high-temperature air bearings, gas turbine seals, low heat dissipation diesel engine piston rings, and cylinder wall lubrication.

**Author Contributions:** Conceptualization, F.Y.; Methodology, F.Y.; Formal analysis, Z.L.; Investigation, Y.Z.; Resources, Y.W.; Writing—original draft, Y.Z.; Writing—review and editing, Y.Z.; Supervision, F.Y. All authors have read and agreed to the published version of the manuscript.

**Funding:** This research was financially supported by the National Natural Science Foundation of China (No. 51975406) and the National Key Research and Development Program (No. 2018YFB1105804).

**Institutional Review Board Statement:** Not applicable.

**Informed Consent Statement:** Not applicable.

**Data Availability Statement:** Data are contained within the article.

**Conflicts of Interest:** The authors declare no conflict of interest.

## References

1. Liu, N.; Liu, Q.; Li, Z.; Bai, Y.; Sun, Y.W.; Li, Z.D. Tribological behavior of plasma-sprayed metal based solid self-lubricating coatings under heavy load. *Wear* **2021**, *486–487*, 204108. [[CrossRef](#)]
2. Kumar, R.; Kumar Banga, H.; Singh, H.; Kundal, S. An outline on modern day applications of solid lubricants. *Mater. Today Proc.* **2020**, *28*, 1962–1967. [[CrossRef](#)]
3. Nguyen, C.; Tieu, A.K.; Deng, G.; Wexler, D.; Vo, T.D.; Wang, L. Tribological performance of a cost-effective CrFeNiAl<sub>0.3</sub>Ti<sub>0.3</sub> high entropy alloy based self-lubricating composite in a wide temperature range. *Tribol. Int.* **2022**, *174*, 107743. [[CrossRef](#)]
4. Bian, S.; Yu, L.; Xu, J.; Xu, J. Impact of Ag on the microstructure and tribological behaviors of adaptive ZrMoN–Ag composite lubricating films. *J. Mater. Res. Technol.* **2022**, *19*, 2346–2355. [[CrossRef](#)]
5. Geng, Y.; Tan, H.; Cheng, J.; Chen, J.; Sun, Q.; Zhu, S. Microstructure, mechanical and vacuum high temperature tribological properties of AlCoCrFeNi high entropy alloy based solid-lubricating composites. *Tribol. Int.* **2020**, *151*, 106444. [[CrossRef](#)]
6. Geng, Y.; Chen, J.; Tan, H.; Cheng, J.; Zhu, S.; Yang, J. Tribological performances of CoCrFeNiAl high entropy alloy matrix solid-lubricating composites over a wide temperature range. *Tribol. Int.* **2021**, *151*, 106912. [[CrossRef](#)]
7. Wang, L.; Zhou, J.; Yu, Y.; Guo, C.; Chen, J. Effect of powders refinement on the tribological behavior of Ni-based composite coatings by laser cladding. *Appl. Surf. Sci.* **2012**, *258*, 6697–6704. [[CrossRef](#)]
8. Liu, J.; Yu, H.; Chen, C.; Weng, F.; Dai, J. Research and development status of laser cladding on magnesium alloys: A review. *Opt. Lasers Eng.* **2017**, *93*, 195–210. [[CrossRef](#)]
9. Zhou, S.H.; Wang, Y.; Jiang, C.; Zhu, J.Z.; Chen, L.Q.; Liu, Z.K. First-principles calculations and thermodynamic modeling of the Ni–Mo system. *Mater. Sci. Eng. A* **2005**, *397*, 288–296. [[CrossRef](#)]

10. Li, F.; Cheng, J.; Zhu, S.; Hao, J.; Yang, J.; Liu, W. Microstructure and mechanical properties of Ni-based high temperature solid-lubricating composites. *Mater. Sci. Eng. A* **2017**, *682*, 475–481. [[CrossRef](#)]
11. Liu, X.B.; Liu, H.Q.; Liu, Y.F.; He, X.M.; Sun, C.F.; Wang, M.-D. Effects of temperature and normal load on tribological behavior of nickel-based high temperature self-lubricating wear-resistant composite coating. *Compos. Part B Eng.* **2013**, *53*, 347–354. [[CrossRef](#)]
12. Li, F.; Cheng, J.; Qiao, Z.; Ma, J.; Zhu, S.; Fu, L. A Nickel-Alloy-Based High-Temperature Self-Lubricating Composite with Simultaneously Superior Lubricity and High Strength. *Tribol. Lett.* **2013**, *49*, 573–577. [[CrossRef](#)]
13. Pinate, S.; Leisner, P.; Zanella, C. Wear resistance and self-lubrication of electrodeposited Ni-SiC: MoS<sub>2</sub> mixed particles composite coatings. *Surf. Coat. Technol.* **2021**, *421*, 127400. [[CrossRef](#)]
14. Liu, F.; Jia, J. Tribological Properties and Wear Mechanisms of NiCr–Al<sub>2</sub>O<sub>3</sub>–SrSO<sub>4</sub>–Ag Self-Lubricating Composites at Elevated Temperatures. *Tribol. Lett.* **2013**, *49*, 281–290. [[CrossRef](#)]
15. Li, J.; Xiong, D.; Wu, H.; Dai, J.; Cui, T. Tribological properties of molybdenized silver-containing nickel base alloy at elevated temperatures. *Tribol. Int.* **2009**, *42*, 1722–1729. [[CrossRef](#)]
16. Huang, X.Y.; Wang, J.H.; Zhang, H.Q.; Ren, J.; Zan, Q.F.; Gong, Q.M.; Wu, B. WC-Ni-Cr-based self-lubricating composites fabricated by pulsed electric current sintering with addition of WS<sub>2</sub> solid lubricant. *Int. J. Refract. Met. Hard Mater.* **2017**, *66*, 158–162. [[CrossRef](#)]
17. Ouyang, J.-H.; Liang, X.-S.; Liu, Z.-G.; Yang, Z.-L.; Wang, Y.-J. Friction and wear properties of hot-pressed NiCr–BaCr<sub>2</sub>O<sub>4</sub> high temperature self-lubricating composites. *Wear* **2013**, *301*, 820–827. [[CrossRef](#)]
18. Feng, S.; Zhou, X.; Zhang, Q. Tribological Behavior of Ni-based Self-lubricating Composites with the Addition of Ti<sub>3</sub>SiC<sub>2</sub> and Ag<sub>2</sub>W<sub>2</sub>O<sub>7</sub>. *J. Wuhan Univ. Technol.—Mater. Sci. Ed.* **2019**, *34*, 698–706. [[CrossRef](#)]
19. Yang, M.S.; Liu, X.B.; Fan, J.W.; He, X.M.; Shi, S.H.; Fu, G.Y. Microstructure and wear behaviors of laser clad NiCr/Cr<sub>3</sub>C<sub>2</sub>–WS<sub>2</sub> high temperature self-lubricating wear-resistant composite coating. *Appl. Surf. Sci.* **2013**, *258*, 3757–3762. [[CrossRef](#)]
20. Cheng, J.; Zhen, J.; Zhu, S.; Yang, J.; Ma, J.; Li, W. Friction and wear behavior of Ni-based solid-lubricating composites at high temperature in a vacuum environment. *Mater. Des.* **2017**, *122*, 405–413. [[CrossRef](#)]
21. Morisada, Y.; Miyamoto, Y.; Takaura, Y.; Hirota, K.; Tamari, N. Mechanical properties of SiC composites incorporating SiC-coated multi-walled carbon nanotubes. *Int. J. Refract. Met. Hard Mater.* **2007**, *25*, 322–327. [[CrossRef](#)]
22. Hareharen, K.; Pradeep Kumar, S.; Panneerselvam, T.; Dinesh Babu, P.; Sriraman, N. Investigating the effect of laser shock peening on the wear behaviour of selective laser melted 316L stainless steel. *Opt. Laser Technol.* **2023**, *162*, 1–13. [[CrossRef](#)]
23. Fan, X.; Li, W.; Yang, J.; Zhu, S.; Cui, S.; Chen, B.; Zhai, H. Effect of MoO<sub>3</sub> Content on Ni<sub>3</sub>Al–Ag–MoO<sub>3</sub> Composite Coating Microstructure and Tribological Properties. *Coatings* **2023**, *13*, 624. [[CrossRef](#)]
24. Gonela, K.K.; Vijayarman, C.; Palanivel, M.; Mariappan, L.; Ramasubramanian, L.N.; Kannan, A.R. Effect of robotic weaving motion on mechanical and microstructural characteristics of wire arc additively manufactured NiTi shape memory alloy. *Int. J. Mater. Res.* **2022**, *114*, 10–11. [[CrossRef](#)]
25. Wang, D.; Tan, H.; Chen, W.; Zhu, S.; Cheng, J.; Yang, J. Tribological behavior of Ni<sub>3</sub>Al–Ag based self-lubricating alloy with Ag<sub>2</sub>MoO<sub>4</sub> formed by high temperature tribo-chemical reaction. *Tribol. Int.* **2021**, *153*, 106659. [[CrossRef](#)]
26. Ye, F.; Lou, Z.; Wang, Y.; Liu, W. Wear mechanism of Ag as solid lubricant for wide range temperature application in micro-beam plasma clad Ni60 coatings. *Tribol. Int.* **2022**, *167*, 107402. [[CrossRef](#)]

**Disclaimer/Publisher’s Note:** The statements, opinions and data contained in all publications are solely those of the individual author(s) and contributor(s) and not of MDPI and/or the editor(s). MDPI and/or the editor(s) disclaim responsibility for any injury to people or property resulting from any ideas, methods, instructions or products referred to in the content.